Front page

Exam information
NFYK10020E - Physics Thesis 60 ECTS, Niels Bohr Institute - Contract:147596 (Qassim Hasan Ali Alnasheet)

Handed in by
Qassim Hasan Ali Alnasheet
bhn696@alumni.ku.dk

Exam administrators
Eksamen Nørre
eksamen-noerre@adm.ku.dk

Assessors
Vitor Cardoso
Examiner
vitor.cardoso@nbi.ku.dk
+4535323769

Marta Orselli
Co-examiner
orselli@nbi.ku.dk

Hand-in information

Title: Environmental effects on the relaxation of black holes
Title, english: Environmental effects on the relaxation of black holes
The sworn statement: Yes
Does the hand-in contain confidential material: No
Did you remember to fill out the AI declaration, which you should upload as an attachment?: Yes

Environmental effects on the relaxation of black holes

Qassim Alnasheet

20 May 2025

Abstract

In 1915, Einstein formulated the general theory of relativity, which describes how massive objects bend and curve the fabric of spacetime. One of the main predictions of general relativity is the existence of black holes, which are dense regions of spacetime in which not even light can escape. Several detections and observations confirm the existence of black holes, including the trajectory of stars in the center of the Milky Way galaxy, the observation by the Event Horizon Telescope, and the direct detection of gravitational waves released from the merger of binary black holes. Black holes emit gravitational waves at certain frequencies when perturbed, and we will explore whether those frequencies change depending on the environment. The results found in this thesis mainly show that the quasinormal modes of the black hole get redshifted when the black hole is placed at the center of a Hernquist-type density distribution. Source-driven oscillations also affect the amplitude at which the power-law decay dominates over the ringdown phase.

Contents

1 Introduction

1.1 The Birth of Gravitational Waves

In the late 17th century, Newton formulated the universal law of gravity. His law was able to describe the trajectory of apples falling from a tree, and the trajectory of planets and stars in the universe. In Newton's formulation, space and time are like a theater stage on which objects like planets and stars move, and the stage does not affect the objects moving through it. Hence, space and time are static and absolute in Newton's formulation.

Later, at the beginning of the 20th century, Albert Einstein formulated the special theory of relativity, which he discovered by studying Maxwell's theory of electromagnetism. According to the special theory of relativity, the speed of light is constant in all inertial frames of reference, and to hold that postulate, Einstein had to reconsider the common notion of space and time. Speed is distance over time, and if the speed of light is constant in all internal frames, distance or space and time must adjust to keep the equality true. Hence, space and time are relative to the observer and not absolute like Newton thought. Einstein not only changed our perspective of space and time but also joined space and time into one entity called spacetime.

Although special relativity successfully resolved the conflict between Newton's theory and Maxwell's theory, which revolved around the speed of light being constant, it remained in conflict with Newton's law of gravitation. According to Newton's law of gravitation, gravity travels at an infinite speed, however, according to special relativity nothing can travel faster than light. Also, Newton does not explain how the Sun exerts the gravitational force on the planets. It took Einstein 10 years to solve this issue, and the solution is known as the general theory of relativity.

In general relativity, spacetime is relative, and massive objects can warp and curve spacetime. For example, the Earth follows the warps and curves in spacetime created by the Sun, and if the Sun suddenly disappears, it would create ripples in the fabric of spacetime which travel at the speed of light, and hence the Earth will not feel the change in gravity before the light from the Sun has reached it. These ripples in spacetime are now called gravitational waves (GWs).

1.2 Astrophysical sources of Gravitational Waves

The first prediction of black holes came from a paper Einstein published in 1916, after Karl Schwarzschild came up with the first exact solution of General Relativity (GR). Schwarzschild's solution is now known describe a non-rotating and non-charged black hole, but at that time, the existence of black holes was still questionable. In electromagnetism, an accelerating charge releases an electromagnetic wave, however, in GR it is not sufficient for a mass to accelerate to release GWs, but it must also accelerate asymmetrically to change the curvature of spacetime. More formally, the second derivative of the quadrupole moment must be non-zero, and the quadrupole moment measures the spherical symmetry of a system, and it is given by

$$Q_{ij} = \int \rho(\vec{x}) \left(x_i x_j - \frac{1}{3}\delta_{ij} x_k x^k \right) \, d^3x, \tag{1.1}$$

with ρ being the mass density, x_i is the spatial coordinate, and in $x_k x^k$ we are summing over the indices using Einstein summation convention. δ_{ij} is the Kronecker delta function which is 1 if $i = j$ and 0 if $i \neq j$. The quadrupole moment is zero for a spherically symmetric distribution [1]. The strain or the strength of a

GW in natural units ($G \equiv c \equiv 1$) is

$$h = \frac{2}{r}\frac{d^2 Q}{dt^2}, \tag{1.2}$$

where r is the distance from the source. The first direct detection of GWs was detected by the LIGO team in 2015, and the GW signal had a peak strain of 10^{-21}. The signal originated from the merger of two binary black holes around 1.3 billion light-years away [2], and this was also the first detection of a black hole merger. The weak strength of GWs make it difficult to detect, but thanks to the advanced sensitivity of the LIGO interferometer, we can now observe GWs consistently. So far, the LIGO detector (along with the Virgo detector) has detected over 200 GW signals originating from binary black hole mergers, neutron star mergers, and black hole and neutron star mergers. Merging binaries fall within LIGO's frequency sensitivity from 10 Hz to 5000 Hz, yet there are many other astrophysical sources of GWs to which LIGO is not sensitive. For example, low-frequency GWs from inspiraling super-massive black holes or GWs from the Big Bang. These low-frequency GWs might be detected through the Cosmic Microwave Background, pulsar timing arrays, or using future space detectors like LISA. Additionally, there are astrophysical sources like (asymmetric) supernovae and X-ray bursts which fall into LIGO's sensitivity but have not been detected yet, and that is probably due to their weak amplitude or unpredictable waveform.

1.3 The Importance of Gravitational Waves

Before the GW detection in 2015, the universe was being observed through photons, neutrinos, and cosmic rays (high-energy protons), and so the detection of GWs opened up a new window into looking at the universe. There some advantages into observing the universe through GWs, for example, unlike photons, GWs can pass through matter without being scattered, and GW detectors are not affected by weather conditions, which could obstruct optical telescopes. GWs are usually easier to detect than neutrinos, and GWs are uncharged thus they do not get deflected by magnetic fields like cosmic rays. There are many applications to observing GWs, including multi-messenger astronomy and testing GR. GWs are especially important when studying black holes, because black holes do not emit any light, and so GWs are the "light" of black holes. The GW signal from the first detection is shown in fig.1, the first phase of the signal from time $= -0.14$ to time $= -0.01$ consists of the inspiral phase, where the black holes spiral into each other and then merge. The frequency of the GW depends on the frequency of the orbit of the black holes, and so the frequency increases until the black holes merge together. At the merger, the maximum amount of energy is released, and it is when the strain is at its peak. After the merger, the ringdown phase dominates, and it is where the black hole relaxes and returns to its ground state. Also, the ringdown phase will be the focus of this thesis. The ringdown is a crucial phase, because according to GR the frequency and the decay rate of the ringdown is purely determined by the mass and spin of the black hole only, and this provides a perfect opportunity to test GR and the no-hair theorem, which states that black holes only have three properties, spin, mass, and electric charge. The ringdown is analogous to the sound heard from a bell after striking it, and the characteristic frequencies at which the black hole oscillates at correspond to the fading notes heard from the bell. These characteristic frequencies are called quasinormal modes (QNMs). Thus, the ringdown consists of different combinations of QNMs. In this thesis, we will explore whether the mass surrounding a black hole can effect its QNMs.

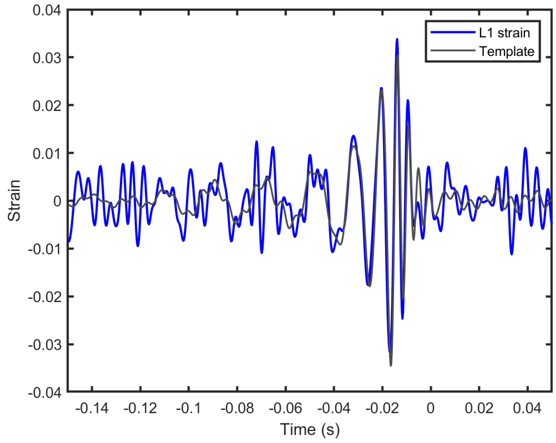

Figure 1: This is a plot of the first GW detection. The blue plot is the signal from the LIGO detector in Livingston, and the grey plot is the predicted waveform used to extract the signal. The time 0 indicates when there is a maximum correlation between the template and the signal. The ringdown phase dominates after the peak strain around time $= -0.01$ [2].

2 Echoes from Black holes

2.1 What is a black hole?

While the philosopher John Michell probably made the first prediction of black holes in the 18th century, the first prediction of black holes as we understand them today came in 1916, when Karl Schwarzschild solved the Einstein field equations. The Einstein field equations are a set of 10 independent equations, relating the curvature of spacetime with the matter or the energy distribution, and it is given by

$$R_{\mu\nu} - \frac{1}{2}Rg_{\mu\nu} + \Lambda g_{\mu\nu} = 8\pi T_{\mu\nu}, \tag{2.1}$$

where $R_{\mu\nu}$ is the Ricci tensor, and it is related to the Riemann curvature tensor. It basically describes how nearby geodesics deviate in a volume of spacetime. $g_{\mu\nu}$ is the metric tensor, and it defines how lengths are measured in a specific geometry, for example, the square of an infinitesimal distance in spacetime is given by

$$ds^2 = g_{\mu\nu}dx^\mu dx^\nu, \tag{2.2}$$

where ds^2 is known as the line element. The metric tensor also defines the dot product between two vectors

$$x^\mu x_\mu = g_{\mu\nu}x^\mu x^\nu. \tag{2.3}$$

The Ricci scalar R is the trace of the Ricci tensor given by

$$R = g^{\mu\nu}R_{\mu\nu}, \tag{2.4}$$

where $g^{\mu\nu}$ is the inverse of the metric tensor $g_{\mu\nu}$ such that

$$g^{\mu\alpha}g_{\alpha\nu} = \delta^\mu_\nu, \tag{2.5}$$

with δ^μ_ν being the Kronecker delta function. The Ricci tensor is related to the Riemann curvature tensor through the inverse metric tensor

$$R_{\mu\nu} = g^{\alpha\beta} R_{\alpha\mu\beta\nu}, \tag{2.6}$$

with $R_{\alpha\mu\beta\nu}$ being the lower-indexed Riemann curvature tensor, and it is directly related to the deviation of geodesics. The Riemann curvature tensor $R^\mu{}_{\nu\alpha\beta} = g^{\mu\sigma} R_{\sigma\nu\alpha\beta}$ is given by

$$R^\mu{}_{\nu\alpha\beta} = \partial_\alpha \Gamma^\mu_{\nu\beta} - \partial_\beta \Gamma^\mu_{\nu\alpha} + \Gamma^\mu_{\rho\alpha}\Gamma^\rho_{\nu\beta} - \Gamma^\mu_{\rho\beta}\Gamma^\rho_{\nu\alpha} \tag{2.7}$$

with

$$\partial_\alpha = \frac{\partial}{\partial x^\alpha}, \tag{2.8}$$

and $\Gamma^\mu_{\nu\alpha}$ is the Christoffel symbol given by

$$\Gamma^\mu_{\nu\alpha} = \frac{1}{2} g^{\mu\beta} \left(\frac{\partial g_{\nu\beta}}{\partial x^\alpha} + \frac{\partial g_{\alpha\beta}}{\partial x^\nu} - \frac{\partial g_{\nu\alpha}}{\partial x^\beta} \right), \tag{2.9}$$

hence in essence the metric tensor is the most important quantity, since the L.H.S. of eq.(2.1) can be rewritten in terms of the metric tensor only.

The cosmological constant Λ was not included in the first publication of GR by Einstein. However, it was later introduced by Einstein to counteract the pull of gravity, because according to GR the universe should collapse because of the attractive force of gravity, but scientists back then thought that the universe was static and unchanging. Thus, the cosmological constant acts as a repulsive force to gravity. Nevertheless, now it is known that the universe is expanding at an accelerating rate, and hence the cosmological constant is indeed required in the Einstein field equations. A positive value of the cosmological constant represents a repulsive force, and it describes the universe we live in. A negative value of the cosmological constant represents an attractive force. The stress-energy tensor $T_{\mu\nu}$ describes the energy content [1].

The first solution of Einstein field equations is known as the Schwarzschild metric, and the line element for the Schwarzschild metric is

$$ds^2 = -a(r)dt^2 + \frac{dr^2}{b(r)} + r^2 d\theta^2 + r^2 \sin^2\theta d\varphi^2, \tag{2.10}$$

where t is the time coordinate, r is the radial distance, θ is the polar coordinate, and φ is azimuthal angle.This is the general form of a spherically symmetric metric, and for the Schwarzschild metric, the functions $a(r)$ and $b(r)$ are given by

$$a(r) = b(r) = \left(1 - \frac{2M_{\mathrm{BH}}}{r}\right), \tag{2.11}$$

with M_{BH} being the mass of the black hole. The Schwarzschild metric has two singularities, one at $r = 0$ which represents the singularity of the black hole, and one at $r = 2M_{BH}$, which represents the event horizon and will be denoted as $r_{\mathrm{h}} = 2M_{\mathrm{BH}}$ [3]. Hence, the Schwarzschild metric describes a non-rotating, uncharged, and static black hole. However, in our universe, black holes are known to have a spin, because black holes are usually formed from stars which have an angular momentum, due to the conservation of angular momentum, the black hole must have a spin. A black hole could have an electric charge, but a black hole with a non-zero electric charge will quickly be neutralized by attracting charged ions. The metric for a spinning black hole is given by the Kerr metric, discovered by Roy Kerr in 1963, and the metric for a charged and non-spinning black hole is given by the Reissner-Nordström metric, discovered in 1916 and 1918. There are many other metrics describing all different types of black holes, however in this thesis we will focus on non-spinning and uncharged black holes, which are described by the Schwarzschild metric (2.10).

2.2 Basic Form of Gravitational Waves

The basic form of a GW can extracted by solving the Einstein field equation in a weak limit, where the self-interaction of GWs can be neglected. The metric tensor in a weak gravitational field can be approximated as

$$g_{\mu\nu}(x) = \eta_{\mu\nu} + h_{\mu\nu}(x), \tag{2.12}$$

where $g_{\mu\nu}(x)$ is a generic metric which depends on the vector $x = x^\mu$, $\eta_{\mu\nu}$ is the Minkowski metric which describes spacetime in the absence of matter. Here we define the Minkowski metric as $\eta_{\mu\nu} = \mathrm{diag}\,(-1, 1, 1, 1)$. $h_{\mu\nu}(x)$ is a small perturbation in spacetime ($|h_{\mu\nu}(x)| \ll 1$). The dot product between vectors is defined in terms of the Minkowski metric

$$x^\mu x_\mu = \eta_{\mu\nu} x^\mu x^\nu, \tag{2.13}$$

and the indices are also raised and lowered using the Minkowski metric

$$h^{\mu\nu} = \eta^{\mu\alpha}\eta^{\nu\beta}h_{\alpha\beta}. \tag{2.14}$$

Then, to a first order approximation, the Chirstoffel symbol can be defined in terms of the perturbed metric

$$\Gamma^\alpha_{\mu\nu} = \frac{1}{2}\eta^{\alpha\beta}\left(\partial_\mu h_{\nu\beta} + \partial_\nu h_{\mu\beta} - \partial_\beta h_{\mu\nu}\right). \tag{2.15}$$

Since we are only considering a first order perturbation, we can neglect the products of the Chirstoffel symbol in the Riemann tensor, because they will be of a second order in the perturbation $h_{\mu\nu}$. Hence, the lower-indexed Riemann tensor simplifies to

$$R_{\alpha\mu\beta\nu} = \frac{1}{2}\left(\partial_\beta\partial_\mu h_{\alpha\nu} - \partial_\nu\partial_\mu h_{\alpha\beta} - \partial_\beta\partial_\alpha h_{\mu\nu} + \partial_\nu\partial_\alpha h_{\mu\beta}\right), \tag{2.16}$$

and the Ricci tensor $R_{\mu\nu} = \eta^{\alpha\beta}R_{\alpha\mu\beta\nu}$ becomes

$$R_{\mu\nu} = \frac{1}{2}\left(\partial_\mu\partial_\rho h_\nu{}^\rho + \partial_\nu\partial_\rho h_\mu{}^\rho - \eta^{\mu\nu}\partial_\mu\partial_\nu h_{\mu\nu} - \partial_\mu\partial_\nu h_\rho{}^\rho\right), \tag{2.17}$$

where

$$h_\nu{}^\rho = \eta^{\rho\sigma}h_{\nu\sigma}, \tag{2.18}$$

and $\eta^{\mu\nu}\partial_\mu\partial_\nu = \Box$ is the *d'Alembet operator*. Eq.(2.17) can be simplified by imposing the following Lorenz gauge

$$\partial^\nu\left(h_{\mu\nu} - \frac{1}{2}\eta_{\mu\nu}h_\rho{}^\rho\right) = 0, \tag{2.19}$$

and thus eq.(2.17) simplifies to

$$R_{\mu\nu} = -\frac{1}{2}\Box h_{\mu\nu}, \tag{2.20}$$

which is L.H.S of the Einstein field equations (2.1). The R.H.S can be found by using the stress-energy tensor to leading order, so it does not depend on the perturbed metric, and this gives Einstein field equations in the weak limit

$$\Box h_{\mu\nu} = 16\pi\left(T_{\mu\nu} - \frac{1}{2}\eta_{\mu\nu}\eta^{\rho\sigma}T_{\rho\sigma}\right). \tag{2.21}$$

This is also known as the linearized Einstein equations. In the absence of matter $T_{\mu\nu} = 0$ or in vacuum, eq.(2.21) becomes

$$\Box h_{\mu\nu} = 0, \tag{2.22}$$

and one possible solution for this relativistic wave equation is

$$h_{\mu\nu} = A_{\mu\nu}\exp\left(ik_\rho x^\rho\right), \tag{2.23}$$

with $A_{\mu\nu}$ being the amplitude of the GW, and $k^\mu = (\omega, k^1, k^2, k^3)$, with ω being angular frequency, and (k^1, k^2, k^3) is the wave number of the GW. In addition to Lorenz gauge (2.19), we can limit $h_{\mu\nu}$ to only spatial perturbations, and we can impose a transverse-traceless gauge

$$h_{0\mu} = 0 \tag{2.24}$$
$$\partial^i h_{ij} = 0 \tag{2.25}$$
$$h_i{}^i = 0. \tag{2.26}$$

Then, for a wave propagating in the z-direction the wave solution becomes

$$h_{ij}\left(t, z\right) = \begin{pmatrix} h_+ & h_\times & 0 \\ h_\times & -h_+ & 0 \\ 0 & 0 & 0 \end{pmatrix}\cos\left(kz - \omega t\right), \tag{2.27}$$

with k being the wave number in the z-direction, and h_+ and $h_\times$ are the two polarizations of the GW [1].

2.3 Ringdown of Black Holes

In GR, the Schwarzschild metric describes a non-rotating black hole, and the Schwarzschild metric is spherically symmetric, and it does not change in time. Thus, a black hole by itself does not create a time-varying quadrupole moment which is necessary for the emission of GWs. Hence, we can consider a small perturbation to the Schwarzschild metric

$$g_{\mu\nu} = g^{(0)}_{\mu\nu} + h_{\mu\nu}, \tag{2.28}$$

where $g^0_{\mu\nu}$ is the Schwarzschild metric, and we can follow a similar process like in section 2.2. However, this process is more complicated in a Schwarzschild background. Thus, we will consider a simpler approach, we will consider a small particle falling into a black hole, such that the mass of the particle is much smaller than the small of the black hole, and the gravitational field of the particle can be ignored. The falling particle will cause the black hole to oscillate, and these oscillations are the QNMs of the black hole. To find the wave equation that grovens the oscillations of the black hole, we will use the least action principle, and we start with Einstein-Hilbert action

$$S_{\mathrm{EH}} = \frac{1}{16\pi}\int d^4x\sqrt{-g}\left(R-2\Lambda\right), \tag{2.29}$$

with g being the determinant of $g_{\mu\nu}$. Here we will assume that $g_{\mu\nu}$ is the Schwarzschild metric given by eq.(2.10). The Einstein-Hilbert action describes how matter and energy affect spacetime, and the Einstein field equations can be obtained by varying this action with respect to the metric tensor. Since we are considering a matter field falling into the black hole, we will also need the action for the matter field

$$S_\phi = \int d^4x\sqrt{-g}\mathcal{L}_\phi, \tag{2.30}$$

where here we will assume that $\mathcal{L}_\phi$ is the Lagrangian for scalar field

$$\mathcal{L}_\phi = -\frac{1}{2}g^{\mu\nu}\partial_\mu\phi\partial_\nu\phi - \frac{1}{2}\mu_0^2\phi^2, \tag{2.31}$$

with $\mu_0 = m\hbar$, and with m being the mass of the scalar field. The first term in the Lagrangian is the kinetic term, and the second term is the potential term. Hence, the total action for the system is

$$S_{\mathrm{total}} = S_{\mathrm{EH}} + S_m \tag{2.32}$$

$$S_{\mathrm{total}} = \frac{1}{16\pi}\int d^4x\sqrt{-g}\left(R-2\Lambda\right) + \int d^4x\sqrt{-g}\mathcal{L}_m. \tag{2.33}$$

The equations of motion for the scalar field can be found by varying the action with respect to ϕ, or by simply using the Euler-Lagrange equation for a general spacetime

$$\frac{\partial\mathcal{L}_m}{\partial\phi} - \nabla_\mu\left(\frac{\partial\mathcal{L}_m}{\partial\left(\partial_\mu\phi\right)}\right) = 0, \tag{2.34}$$

here the covariant derivative ∇_μ for a scalar field is just $\nabla_\mu\phi = \partial_\mu\phi$. Inserting the Lagrangian for the scalar field (2.31) into the Euler-Lagrange equation (2.34) gives

$$-\mu_0^2\phi + \partial_\mu\left(g^{\mu\nu}\partial_\nu\phi\right) = 0 \tag{2.35}$$

$$-\mu_0^2\phi + \left(\partial_\mu g^{\mu\nu}\partial_\nu\phi + g^{\mu\nu}\partial_\mu\partial_\nu\phi\right) = 0 \tag{2.36}$$

$$\nabla^\mu\nabla_\mu\phi - \mu_0^2\phi = 0, \tag{2.37}$$

which is the Klein-Gordon equation. (2.37) can be rewritten in a more convenient form by using the relation

$$\Gamma^\mu_{\mu\nu} = \frac{1}{\sqrt{-g}}\partial_\nu\sqrt{-g}, \tag{2.38}$$

and this will allow us to write the Klein-Gordon equation as

$$\frac{1}{\sqrt{-g}}\partial_\mu\left(\sqrt{-g}g^{\mu\nu}\partial_\nu\phi\right) - \mu_0^2\phi = 0. \tag{2.39}$$

This form will be useful when separating the variables of the scalar field. Now varying the total action (2.33) with respect to $g_{\mu\nu}$ will give us the Einstein field equations. First, the variation of the Einstein-Hilbert action will consist of a variation of $\sqrt{-g}$, Ricci scalar, and the cosmological constant

$$\delta\left(\sqrt{-g}\right) = \frac{1}{2}\sqrt{-g}g_{\mu\nu}\delta g^{\mu\nu} \tag{2.40}$$

$$\delta R = R_{\mu\nu}\delta g^{\mu\nu} + g_{\mu\nu}\Box\delta g^{\mu\nu} - \nabla_\mu\nabla_\nu\delta g^{\mu\nu} \tag{2.41}$$

$$\delta\left(-2\Lambda\right) = -\Lambda g_{\mu\nu}\delta g^{\mu\nu}, \tag{2.42}$$

where the d'Alembert operator is defined in terms of the covariant derivative $\Box = \nabla^\mu\nabla_\mu$. Varying the matter field with respect to the metric tensor will give us the stress-energy tensor $T_{\mu\nu}$

$$\delta\left(\sqrt{-g}\right)\mathcal{L}_m + \sqrt{-g}\delta\left(\mathcal{L}_m\right) = -\frac{\delta\left(\sqrt{-g}\mathcal{L}_m\right)}{\delta g^{\mu\nu}}\delta g^{\mu\nu} \tag{2.43}$$

$$= \sqrt{-g}\left(\frac{1}{2}T_{\mu\nu}\right)\delta g^{\mu\nu}, \tag{2.44}$$

where the stress-energy tensor is defined here as

$$T_{\mu\nu} = -\frac{2}{\sqrt{-g}}\frac{\delta\left(\sqrt{-g}\mathcal{L}_m\right)}{\delta g^{\mu\nu}}, \tag{2.45}$$

which describes the scalar matter content. Inserting these variations in total action (2.33) gives

$$\delta S_{\text{total}} = \int d^4x\sqrt{-g}\left[\frac{1}{16\pi}\left(R_{\mu\nu} - \frac{1}{2}g_{\mu\nu}R + \Lambda g_{\mu\nu}\right) - \frac{1}{2}T_{\mu\nu}\right]\delta g^{\mu\nu} = 0. \tag{2.46}$$

For δS_{total} to be equal to zero, implies that

$$R_{\mu\nu} - \frac{1}{2}Rg_{\mu\nu} + \Lambda g_{\mu\nu} = 8\pi T_{\mu\nu} \tag{2.47}$$

which are the Einstein field equations. For a spherically symmetric metric, the scalar field can be decomposed into radial and angular components. This suggests the following ansatz

$$\phi\left(t, r, \theta, \varphi\right) = \sum_{\ell=0}^{\infty}\sum_{m=-\ell}^{\ell}\frac{\Psi_{\ell m}(r)}{r}Y_{\ell m}\left(\theta\right)e^{-i\omega t}e^{i\omega\varphi}, \tag{2.48}$$

where $\Psi_{\ell m}$ is radial part of the solution, $Y_{\ell m}$ are the spherical harmonics, ℓ is the orbital number, and m is the magnetic quantum number [4, 5]. To get the wave equation for Ψ, we can insert the ansatz (2.48) into the Klein-Gordon equation (2.39), and we find

$$\begin{aligned}
&-\frac{e^{i(-\omega t+m\varphi)}}{a(r)r^3}\Big[-a(r)\Psi_{\ell m}(r)Y''_{\ell m}(\theta) - b(r)a(a)Y_{\ell m}(\theta)\Psi''_{\ell m}(r)r^2 \\
&-\frac{1}{2}\left(Y_{\ell m}(\theta)r^2\Psi_{\ell m}(r)\partial_r\left(a(r)b(r)\right)\right) + \Psi_{\ell m}(r)\left(\frac{1}{2}b(r)a'(r)Y_{\ell m}(\theta)r\right. \\
&\left.+\frac{1}{2}a(r)b'(r)Y_{\ell m}(\theta)r - \cot\theta Y_{\ell m}(\theta)a(r) + \left(\left(m^2\csc^2\theta + r^2\mu_0^2\right)a(r) - r^2\omega^2\right)Y_{\ell m}(\theta)\right)\Big].
\end{aligned} \tag{2.49}$$

The differential equation can be simplified further by replacing $Y_{\ell m}$ with the Legendre polynomials which satisfy

$$\frac{1}{\sin\theta}\partial_\theta\left(\sin\theta\partial_\theta P_{\ell m}\right) - \frac{m^2}{\sin^2\theta}P_{\ell m} = -\ell(\ell+1)P_{\ell m}, \tag{2.50}$$

and by using tortoise coordinates defined as

$$\frac{dr}{dr_*} \equiv \sqrt{a(r)b(r)}, \tag{2.51}$$

where $a(r)$ and $b(r)$ are given by eq.(2.11). Now, eq.(2.49) becomes

$$\frac{d^2\Psi_l}{dr_*^2} + \left[\omega^2 - V_0\right]\Psi_l = 0 \tag{2.52}$$

where V_0 is the Regge-Wheeler potential for a scalar field of mass μ_0,

$$V_0 = a(r)\mu_0^2 + a(r)\frac{\ell(\ell+1)}{r^2} + \frac{\partial_r\left(a(r)b(r)\right)}{2r}. \tag{2.53}$$

The master wave can be rewritten in the time domain by ω^2 with the time derivative because the general solution in the frequency domain has the form

$$\Psi(t,r) = e^{-i\omega t}\Psi(r). \tag{2.54}$$

Thus, eq.(2.52) in the time domain becomes

$$-\frac{\partial^2\Psi_l}{\partial t^2} + \frac{\partial^2\Psi_l}{\partial r_*^2} - V_0\Psi_l = 0, \tag{2.55}$$

and this is known as the Regge-Wheeler equation, which describes of the black hole responses to axial (odd-parity) perturbations. There is a similar equation that governs polar (even) perturbations, but in this thesis, we will only consider axial perturbations. We have omitted the subscript m because it does not depend on the orbital number. In a Schwarzschild background, the potential V_0 is given by

$$V_{\text{SCH.}} = a(r)\left(\mu_0^2 + \frac{\ell(\ell+1)}{r^2} + \frac{2M_{\text{BH}}}{r^3}\right). \tag{2.56}$$

The Regge-Wheeler potential for a vector and a gravitational field can be derived by choosing an appropriate ansatz, however, we will only state the potential for a general massless field in a Schwarzschild background without proofing it

$$V_s = a(r)\left(\frac{\ell(\ell+1)}{r^2} + \frac{2M_{\text{BH}}\left(1-s^2\right)}{r^3}\right), \tag{2.57}$$

with s being the spin of the field [4, 5]. Now, the solutions of the Regge-Wheeler equation that are purely outgoing-wave at infinity, and purely ingoing at the event horizon are the QNMs of the black hole [6].

2.4 The Regge-Wheeler Potential

The Regge-Wheeler potential is probably the most important quantity in the Regge-Wheeler equation, and it can be thought of as a scattering potential, where a wave can either be transmitted or reflected by the potential. The shape of the potential is mainly affected by the mass of the black hole and the orbital number. For $M_{\text{BH}} = 1$, the potential usually has a maximum around the light ring $r = 3$ as shown in fig.2, and goes to zero at infinity (for all black hole masses). Although the Regge-Wheeler potential is mathematically defined inside the black hole, fig.2 only shows the values outside the event horizon because the boundary conditions for ingoing and outgoing waves do not hold (or have to be reconsidered) inside the event horizon, and the boundary conditions are necessary for the computation of the QNMs of the black hole. In the next section, we will explore how a mass surrounding a black hole can affect the Regge-Wheeler potential, and in return affect the QNMs of the black hole.

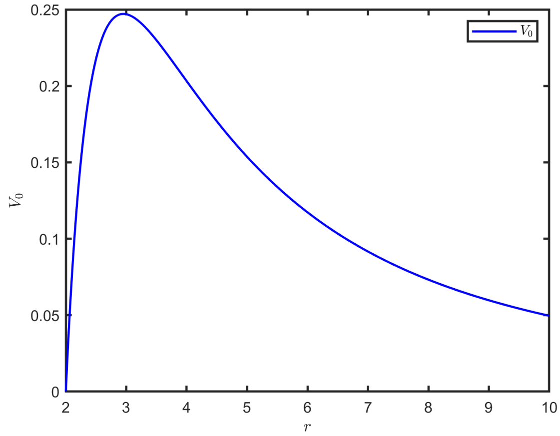

Figure 2: This a plot of the Regge-Wheeler potential (2.57) near the event horizon for a scalar field ($s = 0$), $\ell = 2$, and $M_{\rm BH} = 1$.

3 Effects of the Environment

The Schwarzschild metric is perfect for describing an isolated black hole, however, black holes that are observed through GWs by LIGO and other detectors do not exist in isolation. Most galaxies are known to have a supermassive black hole at their center, and dark matter is also known to cluster around black holes [7]. QNMs are the fingerprints of black holes, and according to the no-hair theorem, all the properties of a black hole can be determined from its QNMs. For this reason, it is important to explore whether the QNMs of a black hole are affected by the environment, and to test how the black hole responds in a non-isolated environment. To model the geometry of a galaxy, we will use a Hernquist density distribution given by

$$\rho_{a_0} = \frac{M_0}{2\pi r(r+a_0)^3}, \tag{3.1}$$

with M_0 being the mass of the halo, and a_0 is a lengthscale that describes the distribution of the matter. Now, to place the black hole at the center of the distribution, we will have to modify the functions $a(r)$ and $b(r)$ in the following way

$$a\left(r\right) = \left(1 - \frac{2M_{\rm BH}}{r}\right)\exp\left(\Upsilon(r)\right), \tag{3.2}$$

$$b(r) = 1 - \frac{2m(r)}{r}, \tag{3.3}$$

where $\Upsilon(r)$ is the redshift given by,

$$\Upsilon(r) = \sqrt{\frac{M_0}{\xi}}\left(2\arctan\left(\frac{r+a_0+M_0}{\sqrt{M_0\xi}}\right) - \pi\right), \tag{3.4}$$

and $\xi = 2a_0 - M_0 + 4M_{\rm BH}$. The mass in function $b(r)$ now depends on both the mass of the black hole and the halo, and it given by

$$m(r) = M_{\rm BH} + \frac{M_0 r^2}{(a_0+r)^2}\left(1 - \frac{2M_{\rm BH}}{r}\right)^2. \tag{3.5}$$

Near the black hole, the mass function $m(r)$ is approximately equal to the mass of the black hole, and at infinity the mass function is approximately $M_{\mathrm{BH}} + M_0$. Now to explore the effect of the environment on the QNMs of the black hole, we can insert the modified functions $a(r)$ and $b(r)$ into the Regge-Wheeler potential given by eq.(2.53), but first we will rewrite $b(r)$ in terms of a new function $B(r)$ defined as

$$B(r) = 1 - 2\left(1 - \frac{2M_{\mathrm{BH}}}{r}\right)\frac{M_0 r}{(a_0 + r)^2}, \tag{3.6}$$

so

$$b(r) = \left(1 - \frac{2M_{\mathrm{BH}}}{r}\right)B(r). \tag{3.7}$$

We also define a new function $K(r)$ given by

$$K(r) = \sqrt{\exp\left(\Upsilon(r)\right)B(r)}. \tag{3.8}$$

These functions will simplify the calculations later [8]. Now using eq.(2.53), we find

$$V_0^{(\mathrm{m})} = a(r)\frac{\ell(\ell+1)}{r^2} + \frac{2M_{\mathrm{BH}}}{2r^3}K(r) + a(r)\frac{\Upsilon'(r)B(r) + B'(r)}{4rK(r)}, \tag{3.9}$$

where the superscript indicates that the potential is for a matter halo, and the subscript indicates that it is for scalar perturbations. We also assumed that the scalar field is massless ($\mu_0 = 0$). The potential for gravitational perturbations can also be found using a different equation, however, we will just state it here without providing a proof

$$V_2^{(\mathrm{dm})} = \frac{a(r)}{r^2}\left(\ell(\ell+1) - \frac{6m(r)}{r} + m'(r)\right), \tag{3.10}$$

where the subscript 2 indicates that the potential is for gravitational perturbations [9].

4 Finding the quasi-normal modes of a black hole

4.1 Hyperboloidal Coordinates

The QNMs of a black hole are found by solving eq.(2.55), but, it will be more convenient to solve it in hyperboloidal coordinates, because it avoids the coordinate singularity at $r_{\mathrm{h}} = 2M_{\mathrm{BH}}$ and at $r = \infty$. The line element in hyperboloidal coordinates $(\tau, \sigma, \theta, \varphi)$ is given by

$$ds^2 = \left(\frac{\lambda}{\sigma}\right)^2 \left\{\Xi\left[-p(\sigma)\,d\tau^2 + 2\gamma(\sigma)\,d\tau d\sigma + w(\sigma)d\sigma^2\right] + \rho(\sigma)^2\,d\omega^2\right\} \tag{4.1}$$

with $\lambda = 2r_{\mathrm{h}}$, and $d\omega^2$ being

$$d\omega^2 = \left(d\theta^2 + \sin^2\theta\,d\varphi^2\right). \tag{4.2}$$

The hyperboloidal functions Ξ, p, γ, w and ρ are given by

$$\Xi = \frac{1}{2} \tag{4.3}$$

$$p(\sigma) = \frac{\lambda}{r_{\rm h}}\sigma^2 \left(1-\sigma\right) \mathcal{K}\left(\sigma\right) \tag{4.4}$$

$$\gamma(\sigma) = 1 - 2\sigma^2 \frac{\mathcal{K}(\sigma)}{\mathcal{K}_{\rm h}} \tag{4.5}$$

$$w(\sigma) = \frac{4r_{\rm h}}{\lambda} \frac{1}{(1-\sigma)\mathcal{K}_{\rm h}} \left(1 - \sigma^2 \frac{\mathcal{K}(\sigma)}{\mathcal{K}_{\rm h}}\right) \tag{4.6}$$

$$\rho(\sigma) = \frac{r_{\rm h}}{\lambda}. \tag{4.7}$$

The function $\mathcal{K}(\sigma) = K(r(\sigma))$ is given by

$$\mathcal{K}(\sigma) = \sqrt{e^{\upsilon(\sigma)}\mathcal{B}(\sigma)}, \tag{4.8}$$

where

$$\upsilon(\sigma) = \Upsilon(r(\sigma)) \tag{4.9}$$

$$= \sqrt{\frac{\mu}{\xi}}\left(2\arctan\left(\frac{2+(\alpha_0-\mu)\sigma}{\sigma\sqrt{\mu\xi}}\right) - \pi\right) \tag{4.10}$$

$$\mathcal{B}(\sigma) = B(r(\sigma)) \tag{4.11}$$

$$= 1 - \frac{4\sigma(1-\sigma)\mu}{(2+\alpha_0\sigma)^2}, \tag{4.12}$$

with $\mu = M_0/M_{\rm BH}$, $\alpha_0 = a_0/M_{\rm BH}$ and $\xi = \xi M_{\rm BH}$. The parameter $\mathcal{K}_{\rm h}$ is the value of the function $\mathcal{K}(\sigma)$ at the horizon ($\sigma = 1$), and it is given by

$$\mathcal{K}_{\rm h} = \mathcal{K}(1) = \exp\left\{\sqrt{\frac{\mu}{\xi}}\left(\arctan\left(\frac{2+(\alpha_0-\mu)}{\sqrt{\mu\xi}}\right) - \frac{\pi}{2}\right)\right\}. \tag{4.13}$$

The hyperboloidal time and radial spatial coordinates are related to the Schwarzschild time and radial coordinates through the following equations

$$t = \lambda(\tau - H(\sigma)) \tag{4.14}$$

$$r = \lambda\frac{\rho(\sigma)}{\sigma}, \tag{4.15}$$

and for our choice of $\rho(\sigma)$ function, r is simply given by

$$r = \frac{r_{\rm h}}{\sigma}. \tag{4.16}$$

Hence, the radial coordinate σ has the domain $[0, 1]$, where $\sigma = 0$ is $r = \infty$ and $\sigma = 1$ is the event horizon $r = r_{\rm h}$. The height function $H(\sigma)$ is constructed in terms of the dimensionless tortoise coordinate $x(\sigma)$ given by

$$x(\sigma) = x_0(\sigma) + x_{\rm h}(\sigma) + x_{\rm reg}(\sigma), \tag{4.17}$$

where x_0 and x_h represent the singular contributions (the contributions from $\sigma = 0$ and $\sigma = 1$), and x_reg represents the regular contributions. Although the explicit form of the function $x_\mathrm{reg}(\sigma)$ might not always be obtainable, the value of x_reg can be always obtained by numerically integrating $dx_\mathrm{reg}/d\sigma$ given by

$$\frac{dx_\mathrm{reg}}{d\sigma} = \frac{r_h}{\lambda}\frac{1}{\sigma^2(1-\sigma)}\left[\frac{\sigma^2}{\mathcal{K}_\mathrm{h}} - \frac{1}{\mathcal{K}(\sigma)} + (1-\sigma)\left(1 + (1+\mu)\sigma\right)\right]. \tag{4.18}$$

The functions x_0 and x_h are given by

$$x_0 = \frac{r_\mathrm{h}}{\lambda}\left[\frac{1}{\sigma} - (1+\mu)\log(\sigma)\right] \tag{4.19}$$

$$x_\mathrm{h} = \frac{r_\mathrm{h}}{\lambda}\frac{\log(1-\sigma)}{\mathcal{K}_\mathrm{h}}. \tag{4.20}$$

Now, the height function can be defined as

$$H(\sigma) = -x_0(\sigma) + x_h(\sigma) - x_\mathrm{reg}(\sigma). \tag{4.21}$$

The Regge-Wheeler equation in hyperboloidal coordinates has the form

$$-w\ddot{\Psi} + p\Psi^{''} + 2\gamma\dot{\Psi}' + \gamma'\dot{\Psi} + p'\Psi' - \bar{V}\Psi = 0, \tag{4.22}$$

where $\dot{\Psi}$ is the derivative with respect to τ, and Ψ' is the derivative with respect to σ. The potential $\overline{V}(\sigma)$ is given by

$$\overline{V}(\sigma) = \frac{\lambda^2}{p(\sigma)}V(r). \tag{4.23}$$

Hence, the scalar potential given by eq.(3.9) in hyperboloidal coordinates is

$$\overline{V}_0^{(\mathrm{m})}(\sigma) = \frac{\lambda}{2M_\mathrm{BH}}\sqrt{\frac{\exp(\upsilon)}{B(\sigma)}}\left[\ell(\ell+1) - \sigma\left(-\mathcal{K}(\sigma) + (1-\sigma)\frac{d\mathcal{K}(\sigma)}{d\sigma}\right)\sqrt{\frac{\exp(\upsilon)}{B(\sigma)}}\right]. \tag{4.24}$$

Similarly, the gravitational potential in hyperboloidal coordinates is

$$\overline{V}_2^{(\mathrm{m})}(\sigma) = \frac{\lambda}{r_\mathrm{h}}\sqrt{\frac{\exp(\upsilon)}{B(\sigma)}}\left(\ell(\ell+1) - \sigma\frac{3m(r(\sigma))}{M_\mathrm{BH}} + \frac{dm(r(\sigma))}{d\sigma}\right). \tag{4.25}$$

4.2 Homogeneous solution

In this section, we will find solutions to the source-free Regge-Wheeler equation (4.22), and those solutions are the natural modes of the black hole that are not influenced by an external particle falling into it. It can be thought of as "striking" the black hole. Although an analytical solution does exist for the Regge-Wheeler equation, the boundary conditions might not actually describe the physical situation we are interested in [10]. Thus, the Regge-Wheeler equation will be solved numerically using the spectral methods described in [11, 12]. We use an initial data of compact support (Gaussian wave-packet) given by

$$\Psi(0,\sigma) = \begin{cases} 0 & \sigma = 0 \\ \dfrac{1}{\lambda_{r_*}\sqrt{2\pi}}\exp\left(-\dfrac{\left(r_*(\sigma) - r_*(\sigma_0)\right)^2}{\lambda_{r_*}^2}\right) & 0 < \sigma < 1 \\ 0 & \sigma = 1 \end{cases} \tag{4.26}$$

$$\dot{\Psi}(0,\sigma) = 0, \tag{4.27}$$

where $r_*(\sigma) = \lambda x(\sigma) = 2r_{\rm h}x(\sigma)$ is the tortoise coordinate, which depends on the mass of the halo, σ_0 is the initial position of the Gaussian, and λ_{r_*} is the width of the Gaussian. The initial data takes the value zero at the event horizon and null infinity, and in all simulations we will assume $M_{\rm BH} = 1$ and $\ell = 2$. The initial data can be thought of as a perturbation in a small region outside the black hole. To test how much the halo affects the QNMs of the black hole, we will compare the angular frequency of different halo configurations with the vacuum state. Also, we will compare the angular frequency we found with the known results. First, we will extract the real part of the angular frequency ω_r by calculating the average distance between the peaks,

$$M_{\rm BH}\omega_r = \sum_j^n \Delta t_{p,j}/(n-j+1), \tag{4.28}$$

where

$$\Delta t_{p,j} = t_{p,j+1} - t_{p,j}, \tag{4.29}$$

and $t_{p,j}$ is the position of the j-th peak. The imaginary part of the angular frequency $\omega_{\rm I}$ is found by fitting the peaks using the following linear equation

$$\log|\Psi_p| = \omega_I t_p + c, \tag{4.30}$$

where Ψ_p is the value of the peak at t_p, and c is the y-intercept.Then we will calculate the following numerical quantity $\delta_{\rm R,I}$, which determines directly how much the black hole frequency deviates from the natural frequency

$$\delta_{\rm R} \equiv 1 - \left|\frac{\omega_{\rm R}}{\omega_{\rm R,s}}\right| \tag{4.31}$$

$$\delta_{\rm I} \equiv 1 - \left|\frac{\omega_{\rm I}}{\omega_{\rm I,s}}\right|. \tag{4.32}$$

Where the subscript s represents the spin. The natural frequencies for spin 0 and $\ell = 2$ are

$$M_{\rm BH}\omega_{\rm R,0} = 0.4836438722 \tag{4.33}$$

$$M_{\rm BH}\omega_{\rm I,0} = 0.09675877598 \tag{4.34}$$

and for spin 2 are

$$M_{\rm BH}\omega_{\rm R,2} = 0.3736716844 \tag{4.35}$$

$$M_{\rm BH}\omega_{\rm I,2} = 0.08896231569 \tag{4.36}$$

[13]. Due to the curvature of spacetime, some of the GWs traveling outwards get scattered by the curved spacetime around the black hole, and this delays the time it takes for the amplitude of GWs to reach zero. The decay of the tail of the ringdown decays according to Price's law

$$\Psi \approx t^{-p}, \tag{4.37}$$

which is a power law, and thus the amplitude of the GWs takes an infinite time to reach zero [14]. The power p can be evaluated by using the following equation

$$p(t) = -t\partial_t \log|\Psi| \tag{4.38}$$

[15]. The time derivative of $\log|\Psi|$ is approximated numerically as

$$\frac{\partial \log|\Psi|}{\partial t} \to \frac{\log|\Psi|_{k+1} - \log|\Psi|_k}{\Delta t}, \tag{4.39}$$

here k is an integer ranging from 1 to the length of the array, and $\Delta t = |(t/M_{\rm BH})_2 - (t/M_{\rm BH})_1|$ is the spacing of the array, which corresponds to the inverse of the sampling frequency $f_s = 1/\Delta t$. Table 1 and Fig.3 show the solution of eq.(4.22), for a scalar perturbation and $\ell = 2$. Fig.3 mainly shows that the environment does not affect the power-law, however, it does affect the decay rate and the frequency of oscillations. The halo causes a redshift in the oscillations of the black hole, and causes the decay rate to decrease as shown in Fig.1. The tail also began at a larger amplitude compared to the vacuum case. These results agree with the results in [9]. Similiar results were found for gravitational perturbations which are shown in table 2 and Fig. 4.

μ	α_0	$M_{\rm BH}\omega_{\rm R}$	$\delta_{\rm R}$	$\lvert M_{\rm BH}\omega_I\rvert$	$\delta_{\rm I}$	$p(t \approx 6000)$
0	0	0.480102	0.007323	0.097069	-0.003206	4.004448
0.1	1	0.466929	0.034561	0.093118	0.037625	4.003083
1	10	0.435093	0.100386	0.086133	0.109815	3.997854
1	100	0.474157	0.019616	0.09615	0.006293	3.988291
10	100	0.426609	0.117927	0.085674	0.114566	3.960853
100	10000	0.474157	0.019616	0.096065	0.007174	2.747862

Table 1: This table shows the quantities extracted from the numerical simulations with the Gaussian initial data for $s = 0$ and $\ell = 2$. The plots are shown in fig.3. The width and position of the Gaussian are $(\lambda_{r_*}, r_0) = (1, 10)$. The numerical parameters are $N_0 = 5$ and $N = 125$, and the temporal array spacing is Δt=0.2667. The power was extracted at $t/M_{\rm BH} = 5999.733$.

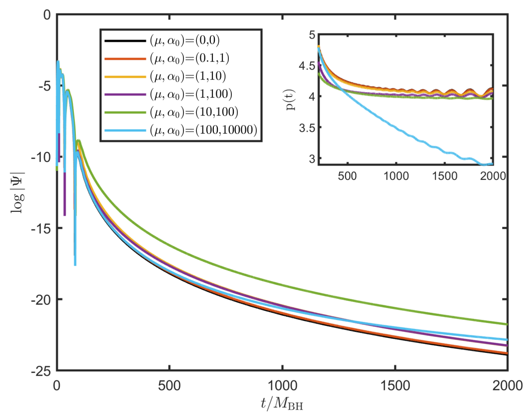

(a)

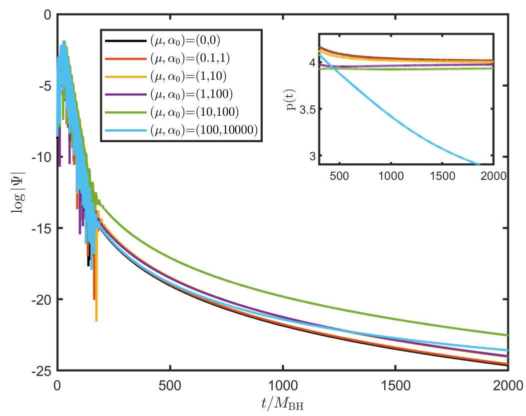

(b)

Figure 3: This figure shows the plots for $s = 0$ and $\ell = 2$ with a Gaussian initial data. The main figure shows the ringdown of the black hole, and the sub-figure shows the local decay rate. Plot (a) is for $(\lambda_{r_*}, r_0) = (10, 10)$, and plot (b) is $(\lambda_{r_*}, r_0) = (1, 10)$. The field was extracted at null infinity.

μ	α_0	$M_{\mathrm{BH}}\omega_{\mathrm{R}}$	δ_{R}	$\lvert M_{\mathrm{BH}}\omega_I\rvert$	δ_{I}	$p(t \approx 6000)$
0	0	0.37173	0.005197	0.089709	−0.008397	4.004506
0.1	1	0.362921	0.028771	0.086354	0.02932	4.003798
1	10	0.341097	0.087174	0.079655	0.104619	3.998304
1	100	0.368155	0.014762	0.08902	−0.000653	3.983264
10	100	0.333666	0.107061	0.078885	0.113273	3.956509
100	10000	0.368155	0.014762	0.088789	0.001944	2.728322

Table 2: This table shows the quantities extracted from the numerical simulations with the Gaussian initial data for $s = 2$ and $\ell = 2$. The plots are shown in fig.4. The width and the position of the Gaussian are $(\lambda_{r_*}, r_0) = (1, 10)$. The numerical parameters are $N_0 = 5$ and $N = 125$, and the temporal array spacing is Δt=0.2667. The power was extracted at $t/M_{\mathrm{BH}} = 5999.733$.

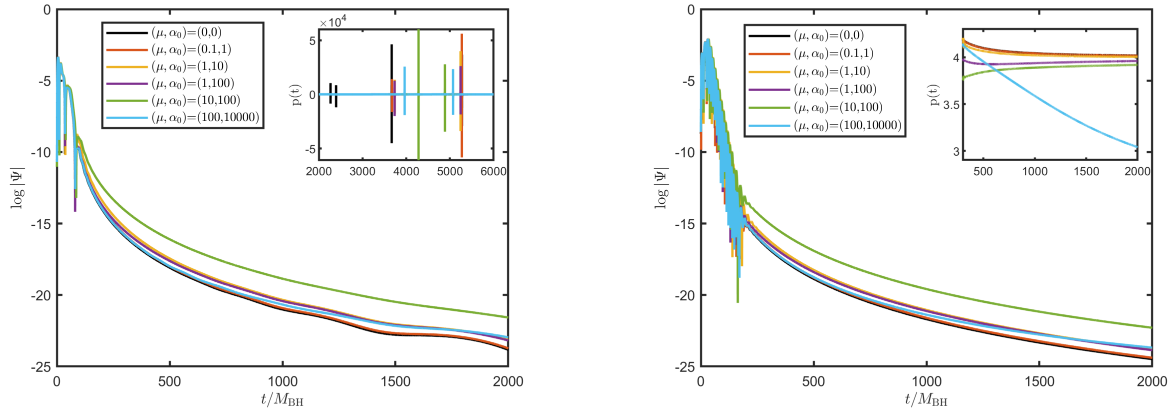

(a) (b)

Figure 4: This figure shows the plots for $s = 2$ and $\ell = 2$ with a Gaussian initial data. The main figure shows the ringdown of the black hole, and the sub-figure shows the local decay rate. Plot (a) is for $(\lambda_{r_*}, r_0) = (10, 10)$, and plot (b) is $(\lambda_{r_*}, r_0) = (1, 10)$. The field was extracted at null infinity.

4.3 Numerical convergence

The relative error in the simulations is calculated using the following equation

$$\epsilon = \left| 1 - \frac{\Psi_N(\tau, 0)}{\Psi_R(\tau, 0)} \right|, \tag{4.40}$$

where the subscript N represents the number of points in the spatial domain used in a simulation, and R is the maximum number of points in the spatial domain used in a simulation.

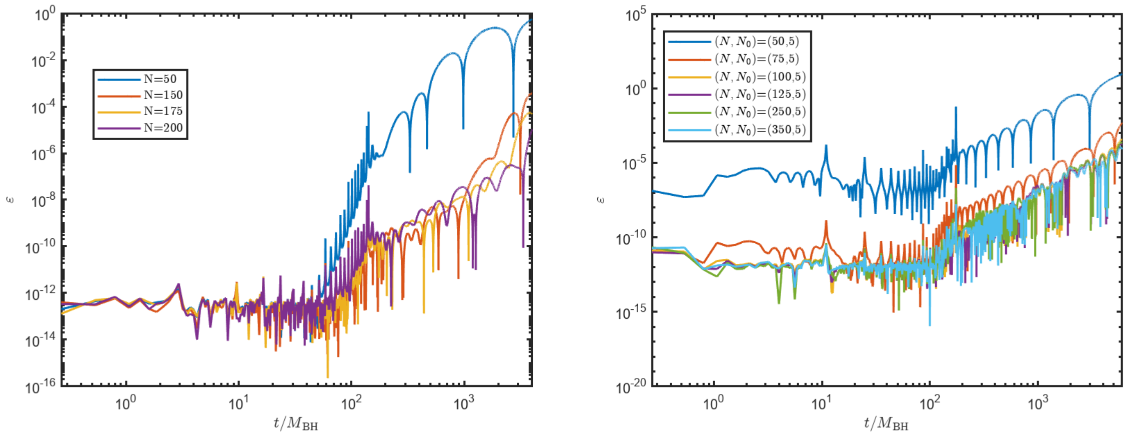

(a) (b)

Figure 5: These plots show the relative error evaluated using eq.(4.40). Plot (a) is for a constant initial data and a reference resolution of $N = 300$. Plot (b) is for a compact support initial data and a reference resolution of $N = 500$. Both plots are for $s = 0$ and $\ell = 2$. The physical parameters are $(\mu, \alpha_0) = (1, 10)$, and the time resolution domain is $N_0 = 5$ for both plots. From these plots, the relative error in the tail is around 10^{-5}.

5 Source-Driven Oscillations

The inhomogeneous Regge-Wheeler equation is given by

$$-\frac{\partial^2 \Psi_l}{\partial t^2} + \frac{\partial^2 \Psi_l}{\partial r_*^2} - V_0 \Psi_l = \mathcal{S}\left(t, r\right), \tag{5.1}$$

where $\mathcal{S}\left(t, r\right)$ is the source term. In hyperboloidal coordinates, it is given by

$$-w\ddot{\Psi} + p\Psi^{''} + 2\gamma\dot{\Psi}' + \gamma'\dot{\Psi} + p'\Psi' - \bar{V}\Psi = \overline{\mathcal{S}}\left(\tau, \sigma\right), \tag{5.2}$$

where the source term in hyperboloidal coordinates is

$$\overline{\mathcal{S}}\left(\tau, \sigma\right) = \frac{\lambda^2}{p(\sigma)} \mathcal{S}\left(t, r\right) \tag{5.3}$$

[8].The solutions of the inhomogeneous Regge-Wheeler equation do not directly correspond to the QNMs of black hole, but they describe how the black hole reacts to non-vanishing external perturbations. Here, we will use a Gaussian source term given by

$$\mathcal{S}\left(t, r\right) = \frac{(1 - 2M_{\rm BH}/r)}{\lambda_x \sqrt{2\pi}} \exp\left(-\frac{\left(x - x_0 + U\tau + A\cos\left(\Omega\tau + \phi\right)\right)^2}{2\lambda_x^2}\right), \tag{5.4}$$

with λ_x being the width of Gaussian, U is the speed of the source term, and x is the dimensionless tortoise coordinate that depends on the mass of the black hole only, and it is given by

$$x(\sigma) = \frac{r_{\rm H}}{\lambda}\left(\frac{1}{\sigma} - \log(\sigma) + \log(1 - \sigma)\right), \tag{5.5}$$

with $\sigma = r_{\rm H}/r$ and $\lambda = 2r_{\rm H}$. The position of the Gaussian is x_0, and τ is the hyperboloidal time. The source term is supposed to mimic a highly eccentric orbit. Fig.6 (left side) shows how the oscillations of the particle cause the tail to start at a larger amplitude, and Fig.7 shows how the halo enhances this effect even further. The right-hand side of Fig.7 shows that for small values of Ω, increasing A causes the tail to start at a lower amplitude, and it also suggests that it has the same effect as changing the initial position of the particle r_0. The left-hand side of Fig. 8 shows the effect of varying Ω while keeping A constant, and it shows that the tail starts at a larger amplitude as Ω increases. The right-hand side of Fig. 8 shows how varying the angle ϕ effects the tail, and it shows that the tail is the longest at $\phi = \pi$. This might be because the cosine function has a minimum at $\phi = \pi$, and this causes the initial position of the particle to increase as can be seen from eq.(5.4).

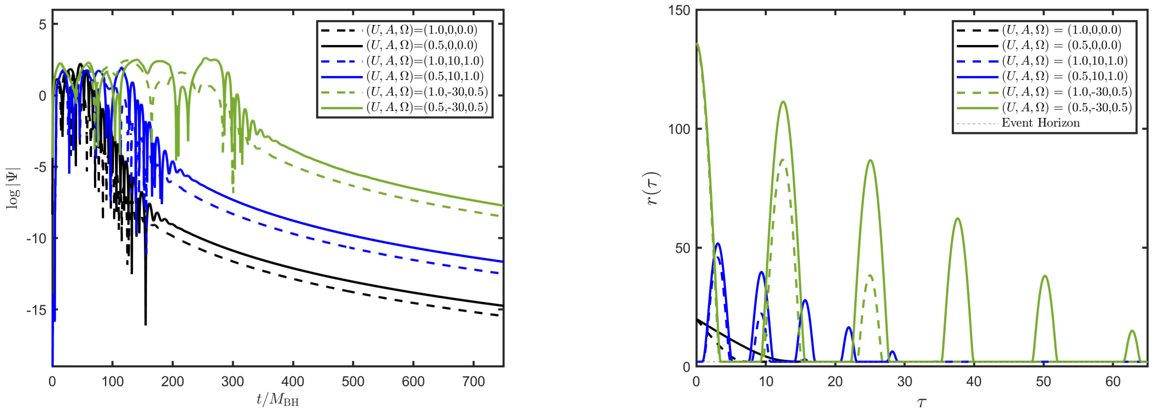

(a) (b)

Figure 6: Plot (a) shows the ringdown in vacuum for different values of A and Ω for $s = 0$ and $\ell = 2$. The dashed lines show the plots for $U = 1$, and the solid lines show the plots for $U = 0.5$. Plot (b) shows the position of the sources in the Schwarzschild coordinate r as a function of the hyperboloidal time τ. Both plots are for $(r_0, \lambda, \phi) = (20, 0.1, 0)$.

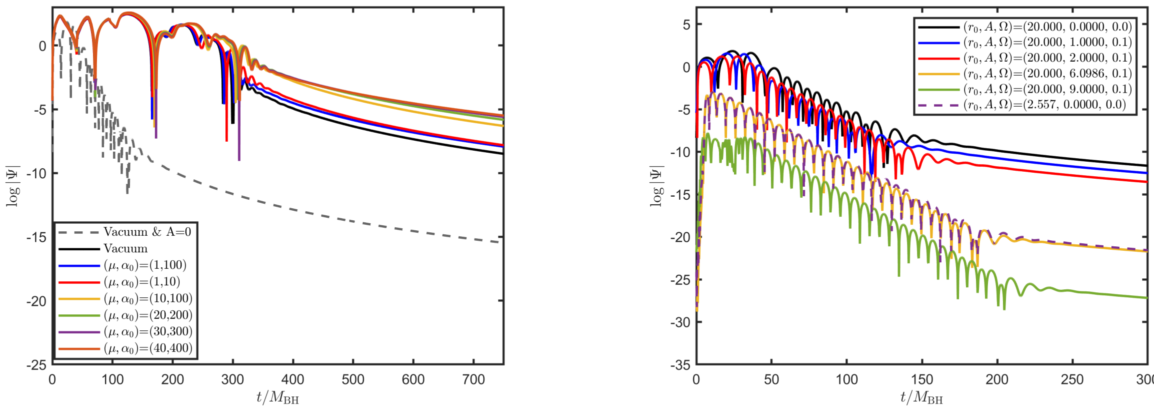

(a) (b)

Figure 7: Plot (a) shows the effect of the halo on the tail for $(A, \Omega) = (-30, 0.5)$ and $(r_0, \lambda) = (20, 0.1)$ (except the grey dashed line is for $A = 0$), where r_0 is the initial position of the Gaussian in Schwarzschild coordinate. Plot (b) shows that for $|\Omega| \ll 1$, increasing A has the same effect as decreasing r_0. Also, it shows that the tail shortens as A increases. Plot (b) shows the ringdown in vacuum only, and both plots are for $s = 0$, $\ell = 2$, $U = 1$, and $\phi = 0$.

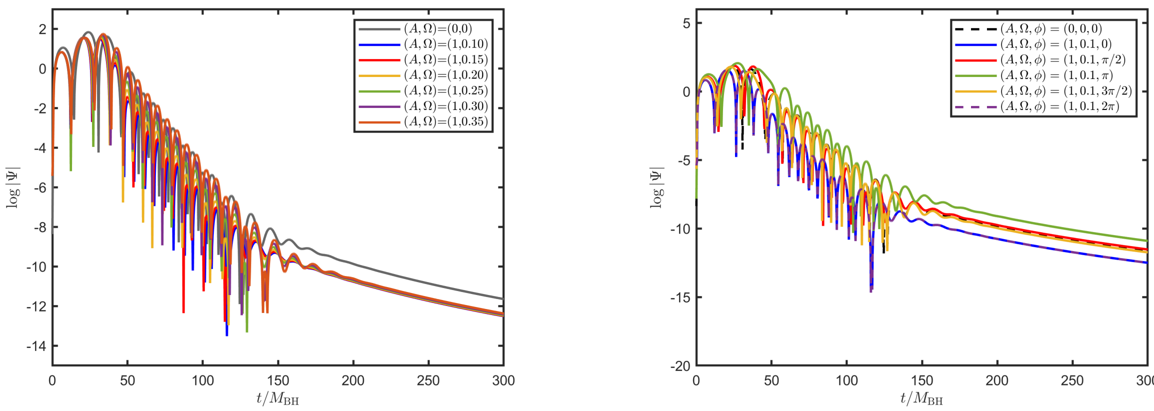

(a) (b)

Figure 8: Plot (a) shows that the tail shortens as Ω increases. Plot (b) shows how varying the angle ϕ affects the tail. Both plots are in a vacuum, and the physical parameters are $s = 0$, $\ell = 2$, and $U = 1$.

6 Conclusion

To conclude, the discovery of GWs changed our view of the universe and allowed us to discover regions of spacetime that cannot be explored using light or other cosmic messengers. Since black holes cannot emit light, GWs act as the light of black holes. Black holes emit gravitational waves at certain frequencies when perturbed, and we discovered that those frequencies change depending on the environment. Mainly, they get redshifted by a factor that depends on the halo configuration. Source-driven oscillations also affect the amplitude at which the power-law decay dominates over the ringdown phase.

References

[1] S. Weinberg, *Gravitation and cosmology : principles and applications of the general theory of relativity.* New York: John Wiley, 1972.

[2] B. A. et al, "Observation of gravitational waves from a binary black hole merger," *Phys. Rev. Lett.*, vol. 116, p. 061102, Feb 2016.

[3] K. Schwarzschild, "On the gravitational field of a mass point according to einstein's theory," 1999.

[4] E. Berti, "A black-hole primer: Particles, waves, critical phenomena and superradiant instabilities," 2014.

[5] E. Berti, V. Cardoso, and A. O. Starinets, "Quasinormal modes of black holes and black branes," *Classical and Quantum Gravity*, vol. 26, p. 163001, July 2009.

[6] L. Rezzolla, "Gravitational waves from perturbed black holes and relativistic stars," 2003.

[7] L. Sadeghian, F. Ferrer, and C. M. Will, "Dark-matter distributions around massive black holes: A general relativistic analysis," *Phys. Rev. D*, vol. 88, p. 063522, Sep 2013.

[8] R. Panosso Macedo, "Hyperboloidal approach for static spherically symmetric spacetimes: a didactical introduction and applications in black-hole physics," *Philosophical Transactions of the Royal Society A: Mathematical, Physical and Engineering Sciences*, vol. 382, Jan. 2024.

[9] V. Cardoso, K. Destounis, F. Duque, R. P. Macedo, and A. Maselli, "Black holes in galaxies: Environmental impact on gravitational-wave generation and propagation," *Phys. Rev. D*, vol. 105, p. L061501, Mar 2022.

[10] P. P. Fiziev, "Exact solutions of regge–wheeler equation and quasi-normal modes of compact objects," *Classical and Quantum Gravity*, vol. 23, p. 2447, mar 2006.

[11] P. Bourg, R. P. Macedo, A. Spiers, B. Leather, B. Béatrice, and A. Pound, "Quadratic quasinormal modes at null infinity on a schwarzschild spacetime," 2025.

[12] R. Panosso Macedo and M. Ansorg, "Axisymmetric fully spectral code for hyperbolic equations," *Journal of Computational Physics*, vol. 276, p. 357–379, Nov. 2014.

[13] E. Berti, "Ringdown - a numerical relativity resource." `https://pages.jh.edu/eberti2/ringdown/`, 2024. Accessed: 2024-11-20.

[14] E. S. C. Ching, P. T. Leung, W. M. Suen, and K. Young, "Late-time tail of wave propagation on curved spacetime," *Phys. Rev. Lett.*, vol. 74, pp. 2414–2417, Mar 1995.

[15] V. Cardoso, G. Carullo, M. De Amicis, F. Duque, T. Katagiri, D. Pereñiguez, J. Redondo-Yuste, T. F. Spieksma, and Z. Zhong, "Hushing black holes: Tails in dynamical spacetimes," *Physical Review D*, vol. 109, June 2024.

Declaration of using generative AI tools (for students)

At the University of Copenhagen, we do our work with ***responsibility*** *and* ***respect for society, cultural heritage, the environment and people*** *around us.*
Integrity, honesty *and* ***transparency*** *are prerequisites for academic work. We expect exam performances to reflect the* ***student's own learning and independent work****.*
Academic work is always based on other people's insights, knowledge and contributions, but always with thorough ***recognition, respect*** *and* ***crediting*** *of this work. This also applies when using generative artificial intelligence.*

Guidelines

Use of generative AI in exams

According to the University's rules for using tools based on generative AI (GAI), you must be transparent about your use of the technology, for example in your methodology section and/or by filling in and submitting the declaration template below as an appendix to your exam papers. When you fill in the declaration, it is important that the reader gets a clear picture of whether and how generative AI has contributed to the final product.

If the template has been chosen as the preferred means of declaration in your course, you must also use it when you have *not* used GAI tools as an aid. In this case, the only thing you need to do is tick the box stating that you have not used generative AI, leaving the rest blank.
By declaring your use of GAI tools, you avoid issues in relation to the rules on exam cheating.

On courses where the use of GAI has been an integrated part of the content, reflection and critical assessment of using GAI may also be included in your exam paper's methodology section. If you are unsure of whether this is the case on your course, you can ask your lecturer or supervisor.

If GAI is the object of your exam paper, its role will appear from your research questions, methodology description, analysis and conclusion. If you also use GAI as an aid in the process, you need to declare it separately.

Points of attention:

- If GAI is a permitted aid on your course, you can use it for dialogue and sparring when writing your exam paper, but you are **not** allowed to let GAI write your paper, even if all aids are permitted.
- If you include GAI material as a source (directly or edited) in your exam paper, the same requirements apply for using quotation marks and source referencing as with all other sources. Otherwise, it will be a case of plagiarism.
- Never feed an AI tool with data that are personally identifiable, protected by copyright or confidential.
- Always remember to check the current rules and guidelines for using GAI at UCPH.
- Read the course description carefully. It's important that you know which aids are permitted on your course. There may be additional documentation requirements, for example that you must describe your key prompts and any source material (what context you have given, what you have fed into the tool, what you have asked the tool to do), describe the output (what responses did the tool give you?), describe the process, for example history and iterations (if you have written back and forth with the tool several times to get a useful output).
- If in doubt, talk to your lecturer or supervisor.

Declaration of using generative AI tools (for students)

☐ **I/we have used generative AI as an aid/tool** *(please tick)*

☒ **I/we have <u>NOT</u> used generative AI as an aid/tool** *(please tick)*

If generative AI is permitted in the exam, but you haven't used it in your exam paper, you just need to tick the box stating that you have not used GAI. You don't have to fill in the rest.

List which GAI tools you have used and include the link to the platform (if possible):

Example: [Copilot with enterprise data protection (UCPH license), https://copilot.microsoft.com]

Describe how generative AI has been used in the exam paper:

1) *Purpose (what did you use the tool for?)*
2) *Work phase (when in the process did you use GAI?)*
3) *What did you do with the output? (including any editing of or continued work on the output)*

Please note: Content generated by GAI that is used as a source in the paper requires correct use of quotation marks and source referencing. Read the guidelines from Copenhagen University Library at KUnet.